Supporting Information

To

Selective Alkane Oxidation by Manganese Oxide: Site Isolation of MnO_x Chains at the Surface of $MnWO_4$ Nanorods

Xuan Li[a,b], Thomas Lunkenbein[a], Verena Pfeifer[a], Mateusz Jastak[a], Pia Kjaer Nielsen[a], Frank Girgsdies[a], Axel Knop-Gericke[a], Frank Rosowski[b,c], Robert Schlögl[a], and Annette Trunschke[a]*

[a]*Department of Inorganic Chemistry, Fritz-Haber-Institut der Max-Planck-Gesellschaft, Faradayweg 4-6, 14195 Berlin, Germany*

E-mail: trunschke@fhi-berlin.mpg.de

[b]*UniCat-BASF Joint Lab, Technische Universität Berlin, Sekretariat EW K 01, Hardenbergstraße 36, 10623, Berlin, Germany*

[c]*BASF-SE, Process Research and Chemical Engineering, Heterogeneous Catalysis, Carl-Bosch-Straße 38, 67056 Ludwigshafen, Germany*

Content

Formatiert: Schriftart: +Überschriften (Cambria)

Formatiert: Schriftart: +Überschriften (Cambria), 12 Pt.

1. Catalyst synthesis

1.1. Starting materials

$Mn(NO_3)_2 \cdot 4H_2O$ (98%, Roth), $Na_2WO_4 \cdot 2H_2O$ (99%, Sigma Aldrich), NaOH (98%, Alfa Aesar), were used as received. Ultrapure water was obtained by using the Milli-Q Synthesis System (MQ). Commercial $MnWO_4$ (ID 18507) used as reference catalyst was purchased from Alfa Aesar (99.9% metal basis, 200 mesh powder), the powder was then pressed and sieved to a particle size of 250-355 µm for catalytic testing.

1.2. Hydrothermal synthesis of nano-structured $MnWO_4$

Nano-structured $MnWO_4$ was synthesized by a method modified from literature.[1] In the first step, an aqueous 0.2 M solution of $Mn(NO_3)_2$ was added to an aqueous 0.2 M solution of Na_2WO_4 while stirring at 295 K. In the second step, 5.8 mL of an aqueous 0.1 M NaOH solution was added to adjust the pH value to 9.9. In the third step, the mixture was transferred to an analytical autoclave HPM-PT-040 (Premex Reactor GmbH), and the temperature was raised from 295 K to 453 K at a rate of 5 K/min. Hydrothermal synthesis was performed at 453 K at autogenous pressure for 12 h. During hydrothermal synthesis the pH was recorded (Figure S10) using a pH probe (ZrO_2 probe Model A2 and Ag/AgCl reference electrode, both with a 1/2“ outer tubing made from C-276; Corr Instruments). In the fourth step, the solid product was separated from the mother liquor by centrifugation, and washed twice with de-ionized water. In the final step, the solid was dried in a muffle furnace in air at 353 K for 12 h. A brownish solid (ID 18942) was collected and thermally treated in argon (flow rate: 50 mL/min) at 673 K for 2 h in a rotating quartz tube to receive the final catalyst (ID 19116).

Formatiert: Schriftart: +Überschriften (Cambria), 12 Pt.

Formatiert: Schriftart: +Überschriften (Cambria), 12 Pt.

1.3. Washing of nano-structured $MnWO_4$ with nitric acid solution

As-prepared $MnWO_4$ (ID 18942) was washed with 2 M solution of nitric acid at 60°C for 1 hour. The solid was separated from the washing solution by centrifugation. The washing solution was analysed by XRF. After centrifugation, the solid was washed with de-ionized water twice and dried in a muffle furnace in air at 353 K for 12 h (ID 20640). Then, the material was thermally treated in argon (flow rate: 50 mL/min) at 673 K for 2 h in a rotating quartz tube to receive the final acid washed catalyst (ID 20655).

1.4. Reference catalysts manganese oxides and VO_x/SiO_2

MnO_2 (ID 18625) with S_{BET}=5.1 m^2/g was achieved by thermal decomposition of $Mn(NO_3)_2 \cdot 4H_2O$ in O_2/Ar at 280°C. Mn_3O_4 (ID 18856) with S_{BET}=11.0 m^2/g was synthesized by mixing $Na_2B_4O_7$ (0.01 mol) and Mn(II)ac_2 (0.01 mol) dissolved in 100 mL milipore water and subsequent addition of a stated amount of aqueous solution of NaOH (0.1 mol) and

then vacuum drying of the mixture. Mn_2O_3 (ID 19405) with S_{BET}=0.5 m^2/g was purchased from Aldrich.

VO_x/SiO_2 (ID 18341) with S_{BET}=377 m^2/g and vanadium loading of 4.1wt.% was prepared by ion exchange, in which an aqueous NH_4VO_3 solution was added to dispersed modified-SBA-15 (ID 18026) functionalized by (3-Aminopropyl) trimethoxysilane (APTMS) in de-ionized water as described before.[2] The catalyst was calcined in a rotating furnace (Xerion Advanced Heating GmbH) at 550°C for 8 h under O_2/Ar (20/80) (500ml/min). For preparation of modified SBA-15, 44.8g of Pluronic P-123 (poly(ethylene glycol)-poly(propylene glycol)- poly(ethylene glycol)) was dissolved in 1.6L of HCl (1.6M), stirred and heated at 35°C in an automated laboratory reactor (LabMax, Mettler-Toledo). After complete dissolution, 85.1g of TEOS were added. After 12h stirring at 35°C, another 45g of TEOS were added. After stirring, the solution was heated in autoclaves at 110°C for 24h. Then, the solid was filtered and washed until the filtrate was neutral. The solid was dried in a furnace at 80°C overnight (ID 18009) and then calcined in two batches at 550°C for 8h under O_2/Ar (20/80) (500ml/min) to obtain the final modified SBA-15 support (ID 18026).

Formatiert: Schriftart: +Überschriften (Cambria), 12 Pt.

Formatiert: Schriftart: +Überschriften (Cambria), 12 Pt.

2. Catalyst characterization

2.1. Electron microscopy

Transmission electron microscopy (TEM) studies were conducted on a Philips CM200 FEG transmission electron microscope operating at 200 kV. High resolution TEM (HRTEM) and high resolution high angle annular dark field scanning transmission electron microscopy (HAADF-STEM) were performed on a Cs corrected FEI TITAN 80-300 operated at 300 kV and a double corrected JEOL JEM-ARM200F equipped with CEOS CESCOR, and CEOS CETCOR hexapole aberration correctors for probe and image forming lenses, respectively, and a cold field emission gun (CFEG). The acceleration voltage was set to 200 kV. TEM samples were prepared by drop deposition from ethanolic suspensions onto lacey-carbon coated Cu grids. Field emission scanning electron microscopy (FESEM) was carried out with a Hitachi S4800 instrument operating at 5 kV.

2.2. X-ray diffraction (XRD) and Rietveld refinement analysis

The X-ray diffraction (XRD) measurement was performed in Bragg-Brentano geometry on a Bruker AXS D8 Advance theta/theta diffractometer, using Ni filtered Cu Kα radiation and a position sensitive LynxEye silicon strip detector. The sample powder was filled into the recess of a cup-shaped sample holder, the surface of the powder bed being flush with the sample holder edge (front loading).

Formatiert: Schriftart: +Überschriften (Cambria), 12 Pt.

Formatiert: Schriftart: +Überschriften (Cambria), 12 Pt.

XRD data were evaluated by whole powder pattern fitting according to the Rietveld method as implemented in the TOPAS software [version 4.2, copyright 1999-2009 Bruker AXS].

During the routine fitting, which uses an isotropic peak width model (i.e. the diffraction profile widths are described as a smooth function of the diffraction angle, independent of hkl), systematic peak profile mismatches of varying degree were observed. With the anisotropic crystallite shape observed by electron microscopy in mind, we developed an appropriate anisotropic (i.e. hkl dependent) peak width model. A model, which worked well, was obtained by modifying the phenomenological model published by Stephens.[3] Due to the macro language implemented in TOPAS, user defined peak models can be implemented easily. The original Stephens model, which was derived to describe anisotropic strain broadening, did not work well with our data. Since we expected anisotropic crystallite size to be the predominant peak broadening factor in our case, we replaced the angular dependent term tan(θ) (representing strain) of the original Stephens model with a cos(θ)-1 (i.e. size) term, while retaining the hkl dependent expression. In addition to a good overall fit, this modified model allowed us to obtain the nominal crystallite size for different crystal directions. The largest dimension was consistently calculated for the 00l direction. Nominal crystallite sizes are reported here for the principal crystal directions h00, 0k0 and 00l (Table S1). It should be noted that such values represent volume weighted average lengths of unit cell columns, LVol-IB. This includes averaging over parallel columns of different lengths within crystallites (shape dependent), as well as averaging over different crystallites of possibly different size (size distribution dependent). Thus, the reported LVol-IB values cannot be directly compared to physical dimensions of discrete crystallites as e.g. observed by electron microscopy. Nevertheless, the XRD derived dimensions may be considered to represent a (volume weighted) average crystallite morphology. To simplify a comparison with the results of other methods, "aspect ratio" D_a/D_b, and D_c/D_b, respectively, were calculated from the principal dimensions in Table S1.

Formatiert: Schriftart: +Überschriften (Cambria), 12 Pt.

Formatiert: Schriftart: +Überschriften (Cambria), 12 Pt.

2.3. Raman spectroscopy

Confocal Raman spectroscopy was performed using a Horiba Jobin LABRAM instrument equipped with a microscope (Olympus). A He-Ne laser (wavelength 632.8 nm, 1.5 mW at the sample position) was used for the excitation. A pressed wafer of the sample was mounted on the sample holder for recording spectrum.

In situ Raman during hydrothermal synthesis was carried out using a Raman probe (RXN1, immersion optics 1/4"OD (HC276); Kaiser Optical Systems). The Raman spectra were automatically recorded every 2 min at a wavelength of 785 nm with an exposure time of 30 s.

2.4. X-ray fluorescence (XRF)

XRF was performed using a Bruker S4 Pioneer X-ray spectrometer. For sample conditioning, beaker of 25 mm diameter with 6 µ MYLAR foil was used to contain 5 ml of

sample solution without any pretreatment. Samples were measured under He atmosphere. The solvent (water) was assumed as matrix and iteratively calculated to sum up the total to 100 %.

2.5. X-ray photoelectron spectroscopy (XPS) and Near edge X-ray absorption fine structure (NEXAFS)

XPS and NEXAFS analyses were conducted at the near ambient pressure XPS end station of the ISISS beamline at HZB/BESSY II (Berlin, Germany). Details of the setup have been published earlier. [4] For the XPS measurements, the kinetic energy of the photoelectrons was varied between 150 eV and 750 eV separately for each core level, hence escape depths (63% of the detected signal stems from this depth) of ca. 0.6 nm (150 eV, denominated as surface) and ca. 1.6 nm (750 eV, denominated as subsurface) were probed. The experiments have been performed at a total pressure of 0.25 mbar in O_2/He or C_3H_8/O_2/He mixtures with a total gas flow of 4.2 sccm at temperatures between 300 °C and 400 °C. The error bar of the absolute elemental composition can be estimated to be 30% due to uncertainties in the monochromatic photon flux, cross sections and peak area determination. However, only the uncertainty in the peak area determination contributes to relative uncertainties in an experimental series (different conditions with the same catalysts or different catalysts under the same condition), and therefore the relative error bar in the XPS figures can be estimated to be approximately 5%. Might be that the roughness of the surface changes as a function of the catalytic conditions (oxidative or reductive). In this case the depth profile will change and therefore the error bar increases.

NEXAFS spectra were recorded simultaneously in total electron yield (TEY) and Auger electron yield (AEY) mode. Due to the low inelastic mean free path of electrons in solids, electron yield X-Ray absorption spectroscopy (XAS) is more surface sensitive than fluorescence based techniques. The highest surface sensitivity of XAS is given in the AEY mode in which Auger electrons on an selected energy interval are analyzed by the spectrometer.[5] In the case of the recorded Mn $L_{2,3}$- edge, electrons with a kinetic energy around 50 eV were analyzed.

2.6. Nitrogen adsorption

The surface area determination was carried out in a volumetric N_2 physisorption set-up (Autosorb-6-B, Quantachrome) at the temperature of liquid nitrogen. The sample was degassed in dynamic vacuum at a temperature of 573 K for 2 h prior to adsorption. The relative N_2 pressure was varied (p/p_0=0.05–0.3), and 11 data points were measured. The linear range of the adsorption isotherm was considered to calculate the specific surface area according to the BET method.

Formatiert: Schriftart: +Überschriften (Cambria), 12 Pt.

Formatiert: Schriftart: +Überschriften (Cambria), 12 Pt.

Formatiert: Schriftart: +Überschriften (Cambria), 12 Pt.

Formatiert: Schriftart: +Überschriften (Cambria), 12 Pt.

2.7. Temperature-programmed oxidation and reduction (TPO-TPR)

TPO was performed in a fixed-bed quartz reactor using 300 mg of the sample. Prior to the first TPO measurement, the sample was pretreated at 400 °C for 2h in Ar (flow rate 50 ml/min, heating rate of 5 °C/min). The TPO measurement was performed up to 400°C in a mixture 0.24% O_2/He (flow rate 100 ml/min), applying a heating rate of 5°C/min and a holding time of 60 min. O_2 consumption was monitored with a paramagnetic detector. After the TPO run, TPR was performed up to 400°C in 0.25% H_2/Ar (flow rate 100 ml/min), applying the same heating rate and holding time. H_2 consumption was monitored with a thermal conductivity detector (TCD). The TCD detector was calibrated by reducing a known amount of CuO. Then the second TPO measurement was done followed by the second TPR run applying the same procedures as in the first runs.

2.8. Catalytic testing of oxidative dehydrogenation of propane (ODP)

The catalytic tests were carried out using a setup for partial oxidation (Integrated Lab Solutions) with 8 fixed bed quartz reactors (6 mm inner diameter) in parallel. Each reactor was equipped with a thermocouple for measuring the temperature inside the catalyst bed containing 300 mg of catalyst previously sieved to a particle size of 250-355 μm and the catalytic performances were determined at atmospheric pressure. The reactant feed comprised the C_3H_8, O_2, and N_2 as diluent passed each reactor at a flow rate of 10 mL/min. The composition of the feed was 10 % C_3H_8, 5 % O_2 and 85% N_2.

The product (and bypass) gas mixtures were analyzed by an online gas chromatograph (Agilent 7890). A system of Plot-Q and Plot-molsieve columns connected to a thermal conductivity detector (TCD) separated the permanent gases CO, CO_2, N_2, O_2, and CH_4. A system of a FFAP and a Plot-Q column connected to a flame ionization detector (FID) allowed the separation of C2-C3 hydrocarbons and oxygenates.

3. Tables

Table S1. Average crystallite sizes D of the particles in the $MnWO_4$ catalyst (ID 19116) along the *a*, *b*, and *c* axis calculated from anisotropic fitting in Rietveld refinement based on the XRD patterns presented in Figure S2.

D_a /nm	D_b /nm	D_c /nm	Ratio D_a/D_b	Ratio D_c/D_b
24.0	17.3	55.4	1.4	3.2

Table S2. Intensity ratio of the peaks at 640 and 641.4 eV in the NEXAFS of nano-structured $MnWO_4$ at the Mn $L_{2,3}$-edge. The spectra in Total Energy Yield (TEY) are presented in Figure S14.

Treatment	Mode[1]	I_{640}	$I_{641.5}$	Peak ratio[2]
O_2/He, n min	TEY	7.67	3.50	2.2
O_2/He, n min	AEY	7.48	4.45	1.7
O_2/He, n min		6.59	3.84	1.7
O_2/He, n min		6.15	3.54	1.7
O_2/He/C3, n min	TEY	8.11	3.59	2.3
O_2/He/C3, n min	AEY	6.97	3.59	1.9
O_2/He/C3, n min		7.14	3.33	2.1
O_2/He/C3, n min		7.32	3.25	2.2

[1] mode of measurement
[2] peak ratio 640/641.5

Table S3. Hydrogen consumption during TPR and oxygen consumption during TPO experiments with nano-structured $MnWO_4$.

	TPO-1	TPR-1	TPO-2	TPR-2
O_2 or H_2 consumption /mmol mol^{-1}	22.1	17.7	7.13	16.6
O_2 or H_2 consumption /10^{-6} mol m^{-2}	2.54	2.03	0.82	1.91
Number of oxygen atoms replenished or reduced[1] /nm^{-2}	3.06	1.22	0.99	1.15
Percentage of surface oxygen atoms replenished or reduced[2] /%	15.3	6.1	5.0	5.8
[1]Assuming that oxidation and reduction only occur at the surface; [2]Assuming a surface oxygen atom density of 20/nm^2				

Table S4. Chemical composition of the washing solution after treatment of nano-structured $MnWO_4$ with nitric acid as determined by XRF.

	MnO	Na_2O	WO_3	H_2O
Concentration /wt %	0.39	0.00	0.00	99.6

Table S5. Surface area and lattice parameters of the nano-structured $MnWO_4$ materials.

	S_{BET}	unit cell parameters			
	/m^2 g^{-1}	*a* /Å	*b* /Å	*c* / Å	*β* /°
As-synthesized $MnWO_4$ nano-rods (ID 18942)	31.0	4.824(1)	5.761(2)	4.998(7)	91.18(2)
Calcined $MnWO_4$ nano-rods (ID 19116)	28.7	4.828(7)	5.762(5)	5.000(7)	91.18(9)
Nitric acid washed and re-calcined $MnWO_4$ (ID 20655)*	29.5	4.828(5)	5.758(8)	4.997(7)	91.18(3)

* The catalyst contains small amounts of an unknown phase.

4. Figures

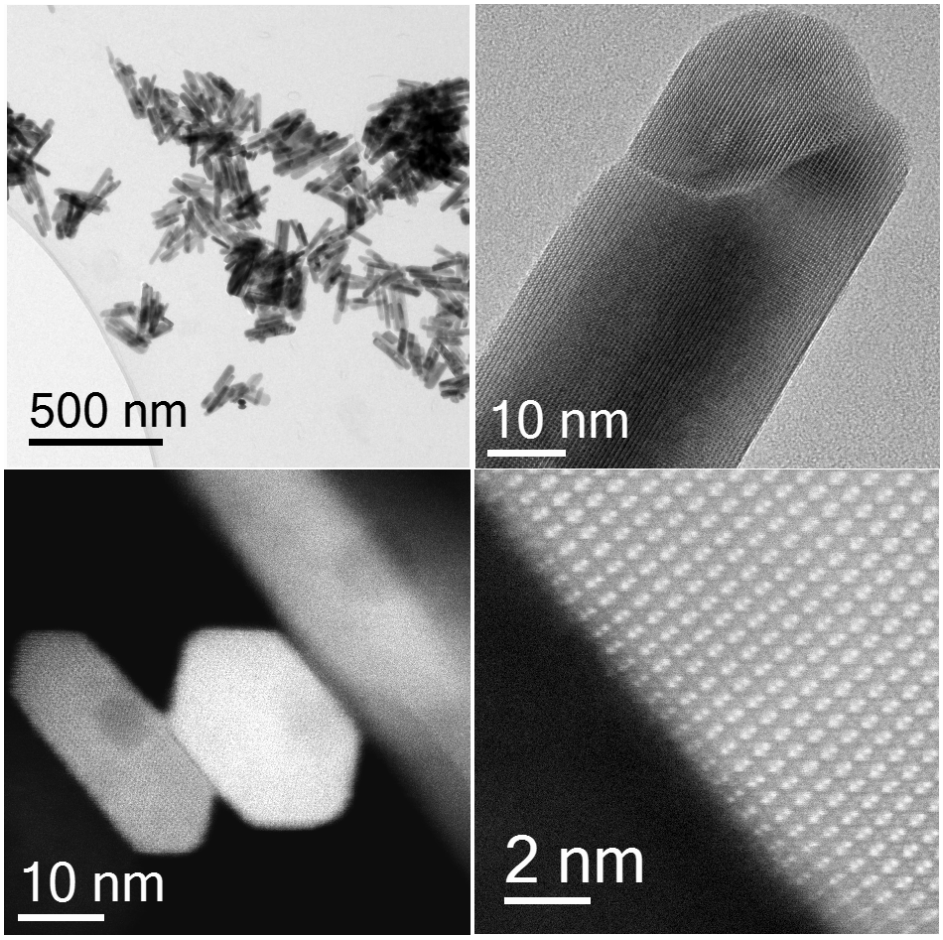

Figure S1. Original images presented in Figure 1.

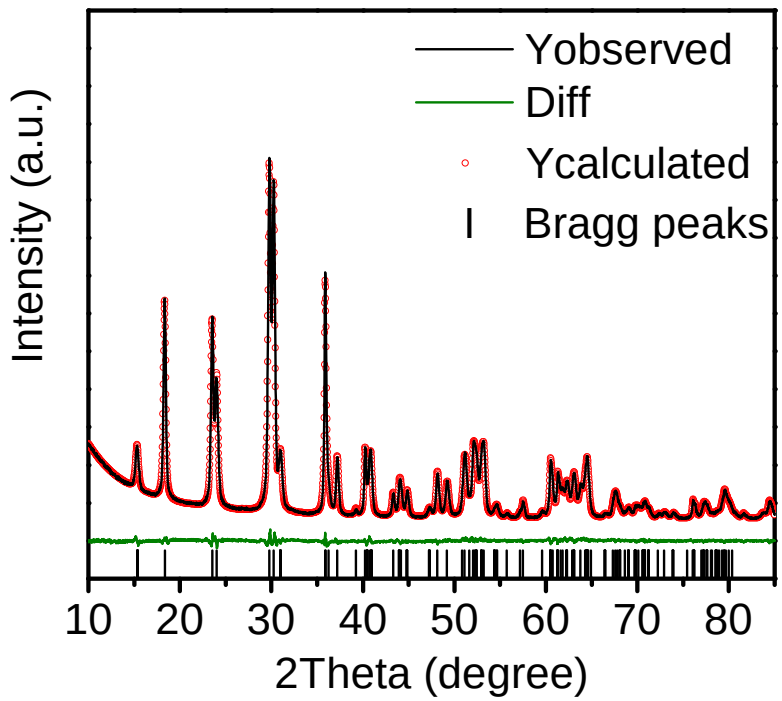

Figure S2. Rietveld refinement of the powder XRD of the $MnWO_4$ catalyst (ID 19116).

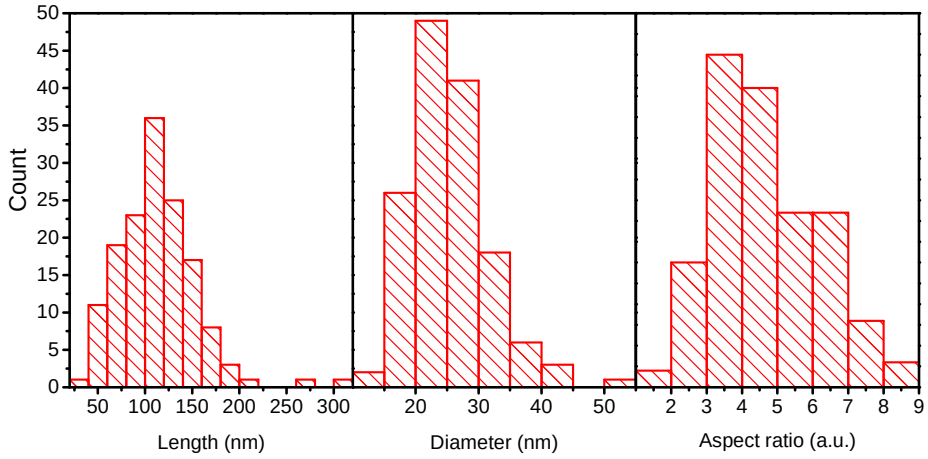

Figure S3. Particle size distribution in the thermally treated nano-structured $MnWO_4$ catalyst (ID 19116) based on the analysis of approximately 146 particles in TEM images (see for example Figure 1a in the main manuscript).

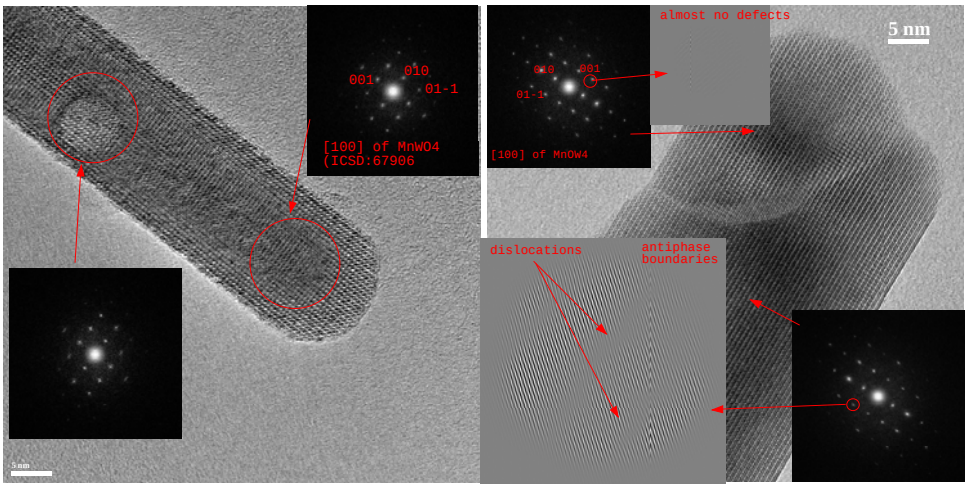

Figure S4. HRTEM images and fast Fourier transform (FFT) analysis of two $MnWO_4$ nanorods in the catalyst (ID 19116).

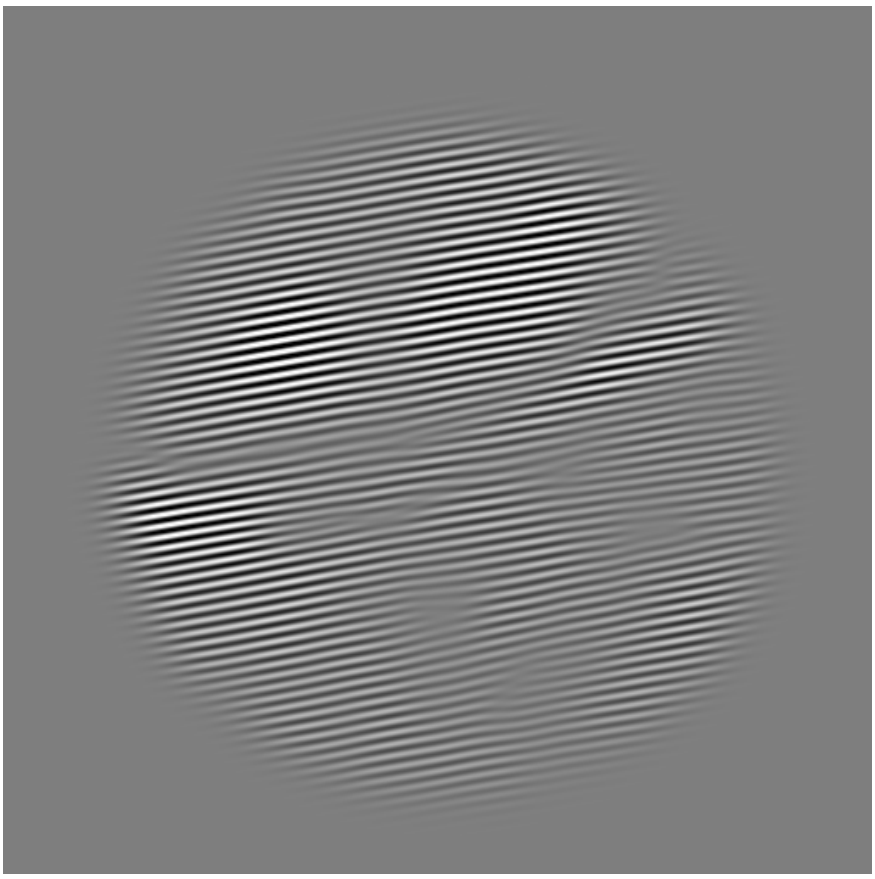

Figure S5. Inverse Fast Fourier transformation (IFFT) of the 110 spots in Figure 1b.

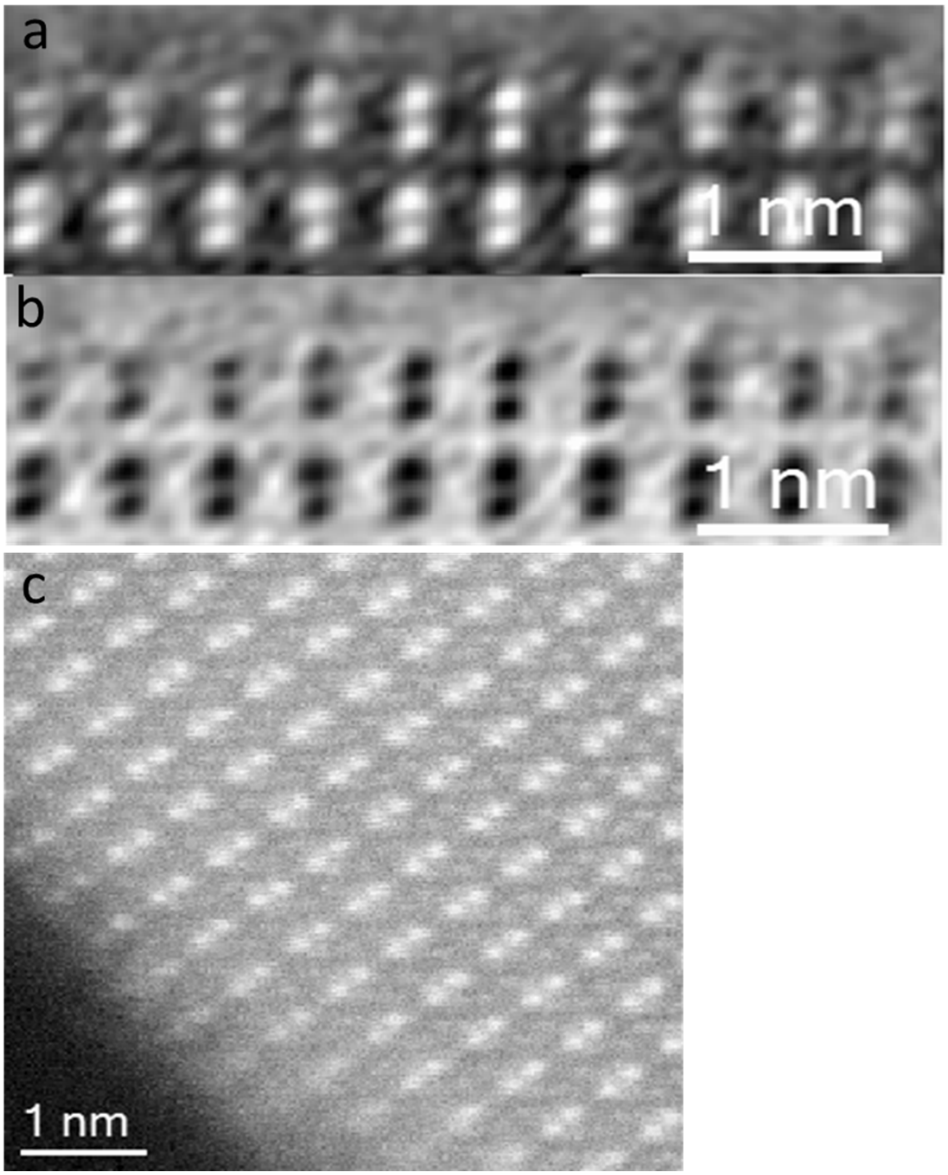

Figure S6. FFT filtered HR-STEM images of $MnWO_4$ (ID 19116) a) HAADF, b) inverted HAADF and c) HR-HAADF-STEM images.

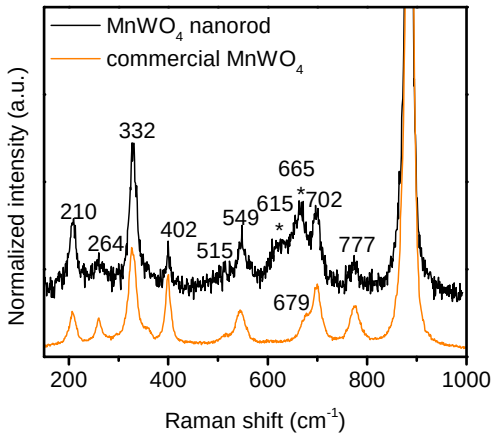

Figure S7. Raman spectrum of the $MnWO_4$ catalyst (ID 19116) (black line) compared to the Raman spectrum of commercial $MnWO_4$ (orange line).

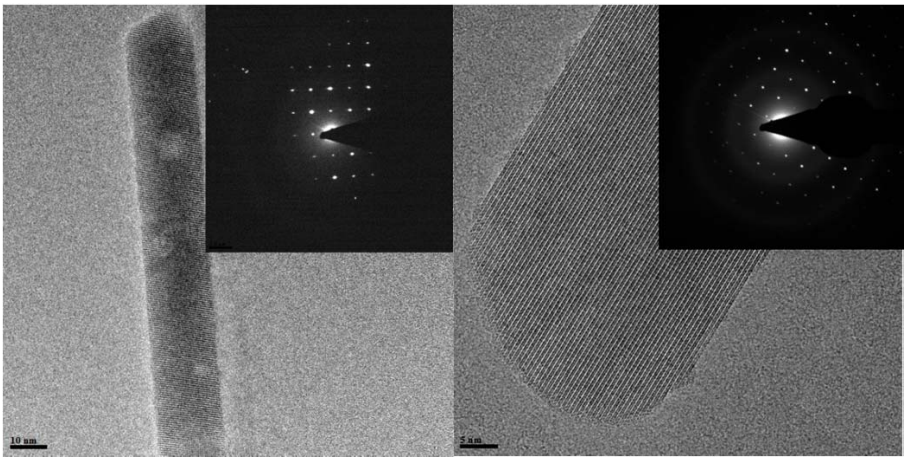

Figure S8. HRTEM images and electron diffraction patterns of $MnWO_4$ nano-rods.

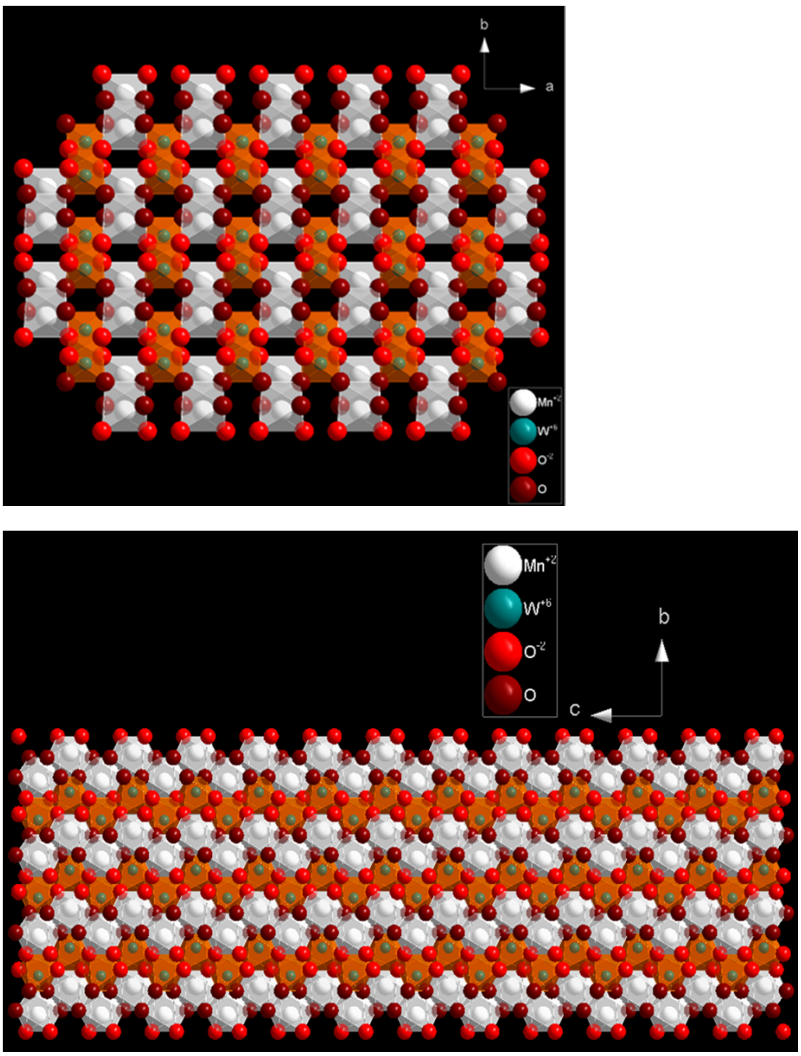

Figure S9. Schematic representation of the crystal structure of $MnWO_4$ viewed along a) the [001] axis and b) the [100] axis. White ball represents Mn^{2+}, green ball represents W^{6+}, red ball represents O^{2-} (bridging oxygen) and wine ball represents terminal oxygen atoms^{-} (tungsten oxygen double bond).

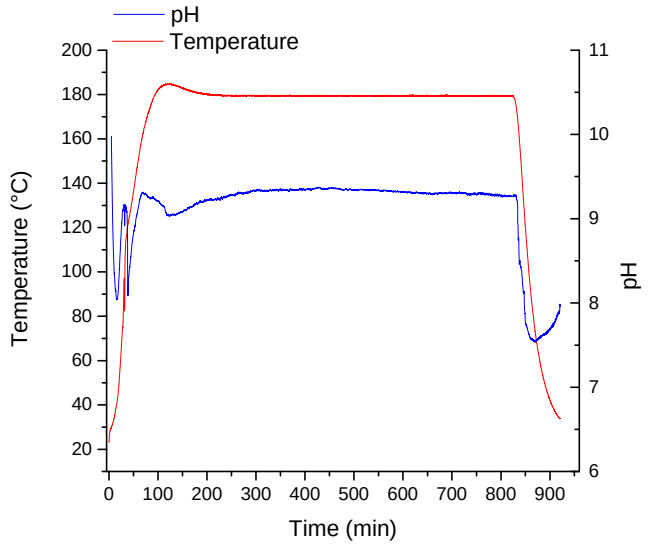

Figure S10. Recorded workflow during hydrothermal synthesis of nano-structured $MnWO_4$; blue line: pH value measured in the autoclave, red line: temperature of the synthesis gel.

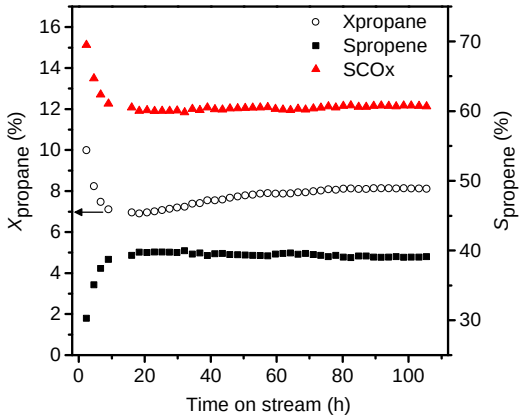

Figure S11. Time on stream plot of propane conversion and selectivity to propene in the oxidative dehydrogenation of propane at T=400°C, and W/F=1.8 g s/ml over nano-structured $MnWO_4$ (catalyst ID 19116); The feed was composed of C_3H_8:O_2:N_2=10:5:85; The changes in the conversion (X) of propane and the selectivity (S) to propylene and carbon oxides (COx: CO + CO_2) are shown with time on stream.

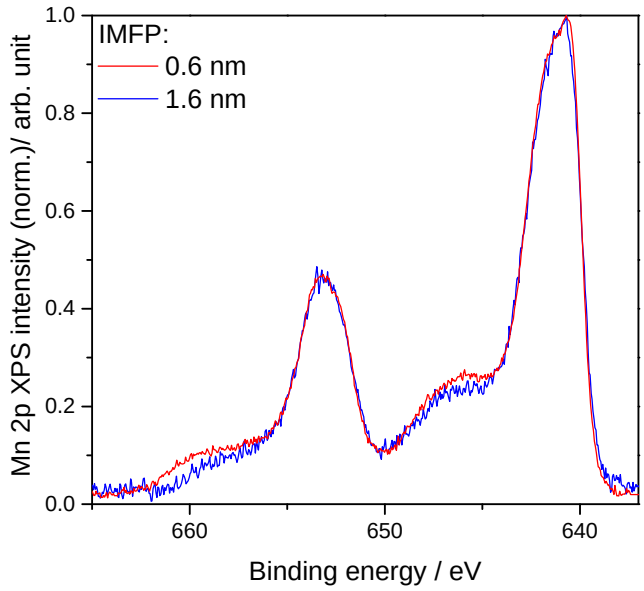

Figure S12. Mn 2p spectra of nano-structured $MnWO_4$ within different detection depths represented by the inelastic mean free path (IMFP) of electrons measured by synchrotron-based NAP-XPS at T=300 °C applying a total pressure of 0.25 mbar O_2 and He flows of 2 and 2.2 sccm, respectively.

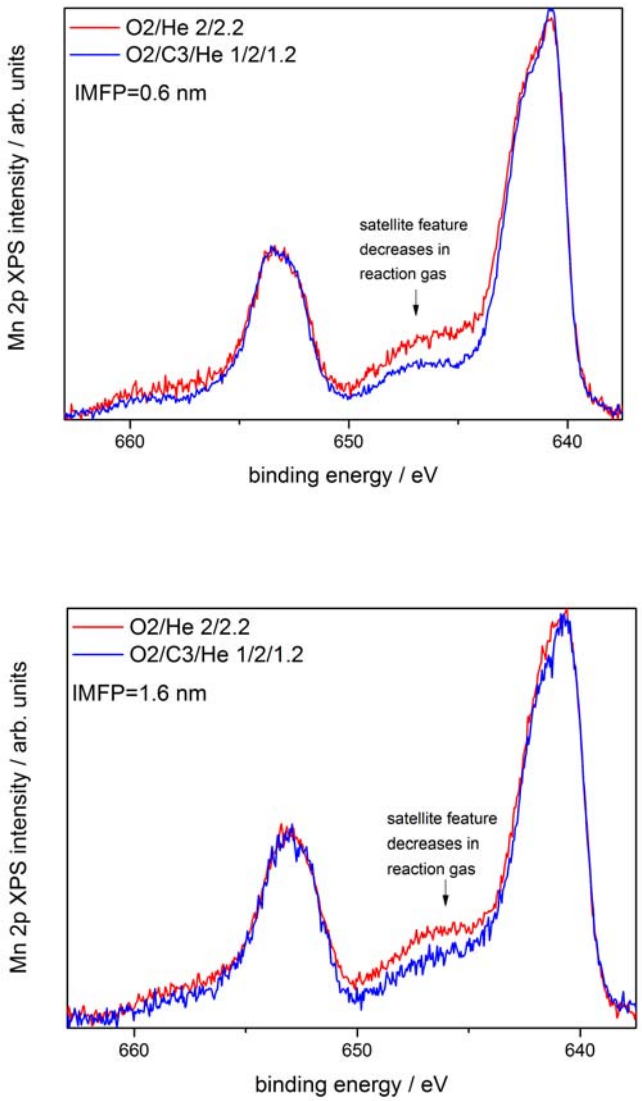

Figure S13. Mn 2p spectra of nano-structured $MnWO_4$ within different detection depths represented by the inelastic mean free path (IMFP) of electrons measured by synchrotron-based NAP-XPS at T=300 °C applying a total pressure of 0.25 mbar under different reaction atmospheres; Red lines: O_2 and He flows of 2 and 2.2 sccm, respectively; Blue lines: O_2, C_3H_8, and He flows of 1, 2, and 1.2 sccm, respectively.

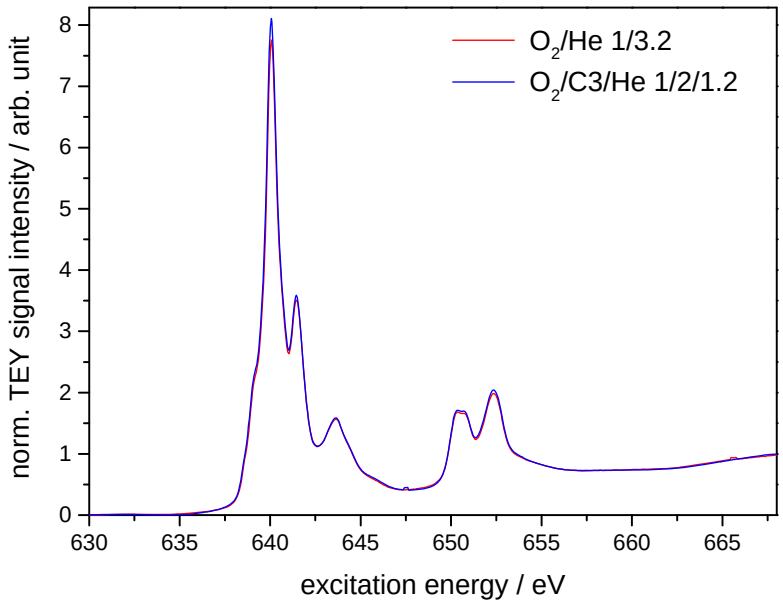

Figure S14. NEXAFS of nano-structured $MnWO_4$ measured at the Mn $L_{2,3}$-edge in total electron yield (TEY) in different reaction atmospheres at T=380°C; Red lines: O_2 and He flows of 1 and 3.2 sccm, respectively; Blue lines: O_2, C_3H_8, and He flows of 1, 2 and 1.2 sccm, respectively.

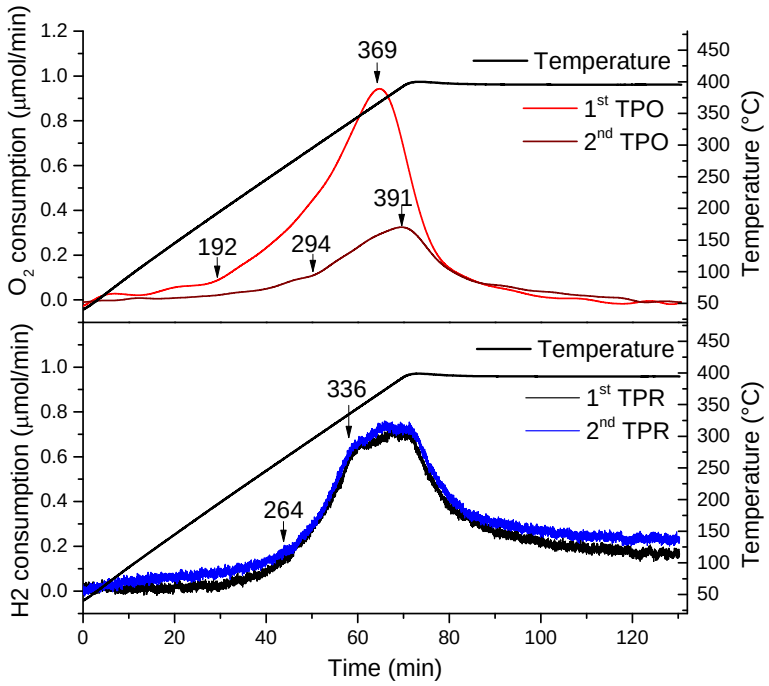

Figure S15. Temperature-programmed oxidation (TPO) (top), and temperature-programmed reduction (TPR) (bottom) profiles of nano-structured $MnWO_4$.

5. References

[1] S.-H. Yu, B. Liu, M.-S. Mo, J.-H. Huang, X.-M. Liu, Y.-T. Qian, *Adv. Funct. Mater.* **2003**, *13*, 639-647.

[2] P. Gruene, T. Wolfram, K. Pelzer, R. Schlögl, A. Trunschke, *Catal. Today* **2010**, *157*, 137-142.

[3] P. Stephens, *J. Appl. Crystallogr.* **1999**, *32*, 281-289.

[4] A. Knop-Gericke, E. Kleimenov, M. Hävecker, R. Blume, D. Teschner, S. Zafeiratos, R. Schlögl, V. I. Bukhtiyarov, V. V. Kaichev, I. P. Prosvirin, A. I. Nizovskii, H. Bluhm, A. Barinov, P. Dudin, M. Kiskinova, in *Advances in Catalysis, Vol. Volume 52* (Eds.: C. G. Bruce, K. Helmut), Academic Press, **2009**, pp. 213-272.

[5] M. Salmeron, R. Schlögl, *Surf. Sci. Rep.* **2008**, *63*, 169-199.

Formatiert: Deutsch (Deutschland)